

Copy 1 of 3
RM L54F04

USR 7884
10 Aug 54

NACA RM L54F04



NACA

RESEARCH MEMORANDUM

49561

THEORETICAL INVESTIGATION BASED ON
EXPERIMENTAL FREQUENCY-RESPONSE MEASUREMENTS OF AN
AUTOMATIC ALTITUDE CONTROL IN COMBINATION WITH A
SUPERSONIC MISSILE CONFIGURATION

By Ernest C. Seaberg, Edward S. Geller,
and William W. Willoughby

Langley Aeronautical Laboratory
Langley Field, Va.

CLASSIFIED DOCUMENT

NATIONAL ADVISORY COMMITTEE
FOR AERONAUTICS

WASHINGTON

August 3, 1954



NATIONAL ADVISORY COMMITTEE FOR AERONAUTICS

RESEARCH MEMORANDUM

THEORETICAL INVESTIGATION BASED ON

EXPERIMENTAL FREQUENCY-RESPONSE MEASUREMENTS OF AN
AUTOMATIC ALTITUDE CONTROL IN COMBINATION WITH A
SUPERSONIC MISSILE CONFIGURATION

By Ernest C. Seaberg, Edward S. Geller,
and William W. Willoughby

SUMMARY

This analysis contains the results of an investigation in which a simple altitude control based on static-pressure and rate-of-climb sensing is combined with a supersonic missile as a servomechanism to yield the closed-loop behavior of the entire system. The results show that the control system can be made to function successfully when applied to a low-altitude missile of the boost-glide type and it is indicated that it would perform satisfactorily at high altitude. It is also probable that the problems encountered with the low-altitude boost-glide missile are more severe than those which would be encountered with a two-stage high-altitude missile which has thrust available for the second stage.

INTRODUCTION

The analytical investigation conducted herein is concerned with the problem of maintaining the flight of a ground-launched canard missile configuration at a predetermined altitude. The purpose of this investigation is to determine the practicability of using a simple system sensitive to static pressure and rate of climb in a low-altitude boost-glide type of missile with the view toward using the results obtained as a guide to future altitude stabilization problems. It is probable that the importance of altitude stabilization will be dictated by certain tactical aspects of long-range missile operation.

For the present investigation a device was constructed which senses altitude variations in terms of atmospheric pressure and rate of change of atmospheric pressure. The output of this device was coupled to a servomotor through a suitable pickoff arrangement. The frequency response

of this combination was obtained experimentally and was used to represent the altitude control in an analytical study which predicts the time history of the missile trajectory from launching to a preselected altitude.

The airframe on which this analysis is based is an all-metal research model of the canard missile type. Reference 1 discusses the results of a previous flight test of the model conducted for the purpose of obtaining aerodynamic stability derivatives. In reference 2 the aerodynamic stability derivatives are tabulated for various flight conditions, and reference 3 presents additional derivatives necessary for a three-degree-of-freedom longitudinal study including changes in forward speed.

SYMBOLS

Z_o	output altitude response, ft
Z_i	input altitude command signal, ft
ϵ	altitude error signal, $Z_i - Z_o$, ft
x	linear servomotor displacement, in.
δ	canard elevator deflection, radians unless otherwise noted
θ	pitch attitude angle, deg
α	angle of attack, deg
γ	flight-path angle, deg
g	acceleration due to gravity, 32.2 ft/sec^2
a_n	normal acceleration, g units
t	time, sec
x_{sm}	static margin, fraction of \bar{c}
\bar{c}	mean aerodynamic chord, 1.776 ft
S	wing area, 4.1 sq ft
M	Mach number

q	dynamic pressure, lb/sq ft
$j = \sqrt{-1}$	
ω	angular frequency, radians/sec
D	differential operator, d/dt
K_{cg}	control gearing ratio, δ/x , radians/in.
KG	transfer function expressed as a linear function of D
$KG(j\omega)$	frequency response
$A(j\omega), B(j\omega)$	polynomial functions of $j\omega$
AR	magnitude of $KG(j\omega)$
PA	phase of $KG(j\omega)$, deg
C_L	lift coefficient, Lift/qS

$$C_{L\delta} = \frac{\partial C_L}{\partial \delta}$$

Abbreviations:

ic	initial condition
db	decibels, $20 \log_{10} AR$

Dot over a symbol denotes derivative with respect to time.

DESCRIPTION OF ALTITUDE CONTROL SYSTEM

Physical Characteristics

A photograph and a schematic diagram of the altitude control are shown in figure 1. The major components of this device are an aneroid pressure sensing element, a rate-of-climb sensing element, a pickoff, and a servomotor. These components function in the following manner:

The altitude error is sensed as a pressure variation through a sealed box containing two bellows, one of which is the aneroid which

serves as the altitude reference, while the other gives a rate signal by means of a capillary and an insulated reservoir. Although the thermal insulation is not shown for the reservoir pictured in figure 1(a), it would be necessary for a flight model of this device to minimize erroneous rate-of-climb signals generated by flight temperature variations. Movement of the bellows is transmitted outside the box by a pivoted bar where it is sensed by an air pickoff (see inset in fig. 1(b)). The pickoff signal is transmitted as a pressure differential across a diaphragm linked to the servo slide valve. At this point the signal is amplified pneumatically by the servo. The servo has position feedback, making it self-centering with its static deflection proportional to the input signal. Presetting the control is achieved by artificially lowering the pressure in the box to correspond to the desired altitude and adjusting the spring load on the pivoted bar until the pickoff centers.

Frequency Responses

Frequency responses of the altitude control obtained experimentally by varying the input pressure to the system sinusoidally over a range of frequencies at sea level are shown in figure 2. Three sinusoidal pressure inputs were used and these were equivalent to altitude inputs of approximately ± 170 feet, ± 320 feet, and ± 530 feet at sea level. The faired curve shown in figure 2 averages the results of these three input amplitudes. In figure 3, this faired curve is compared with the frequency-response plot of the analytical transfer function

$$\frac{x}{\epsilon} = \frac{2.24(D + 0.16)}{(D + 1.16)(D^2 + 119D + 5480)}$$

which was obtained by curve-matching techniques and was used for portions of this analysis for which completely graphical solutions could not readily be obtained. The method of approximating the autopilot transfer function by curve-matching techniques has been used previously in the analysis of a nonlinear attitude control (see discussion of figs. 16 and 17 in ref. 4).

A further examination of the altitude-control transfer function x/ϵ indicates that the lead term has a break frequency of 0.16 radian per second compared with 1.16 radians per second for the linear lag term. The denominator quadratic has an undamped natural frequency of 74 radians per second and a critical damping ratio of about 0.8. It is pointed out later in the results that the two-degree-of-freedom airframe transfer function Z_0/δ contains a double integration and does not contribute any dynamic lead. The dynamic lead necessary for stability therefore must come from the controlling elements or more precisely from the

rate-of-climb sensing element. It is obvious that the lead term in the aforementioned transfer function x/ϵ is closely related to the rate-of-climb dynamics and that the linear lag term is related to the aneroid dynamics. It is quite evident then that, in order to obtain the lead required for stability, the break frequency of the numerator term must be low compared with the break frequencies of the balance of the system dynamics including the airframe dynamics. The model of the altitude control (fig. 1) was therefore designed so that certain physical variations were possible (namely, the size of the capillaries, the size of the reservoir, the size of the bellows, the spacing of the bellows to vary the relative amount of rate or displacement signal, the pickoff pressure, and the centering-spring constant). Frequency-response measurements were then obtained for several combinations of these physical variations. The end result of this experimental investigation was the frequency response presented in figure 2, for which sufficient lead for stability over the broadest band of frequencies was obtained. Therefore in the analysis of the overall system stability, the gain adjustment will be less critical when the controlling elements are represented by the frequency response shown in figure 2 than for any of the other system frequency responses measured in the laboratory.

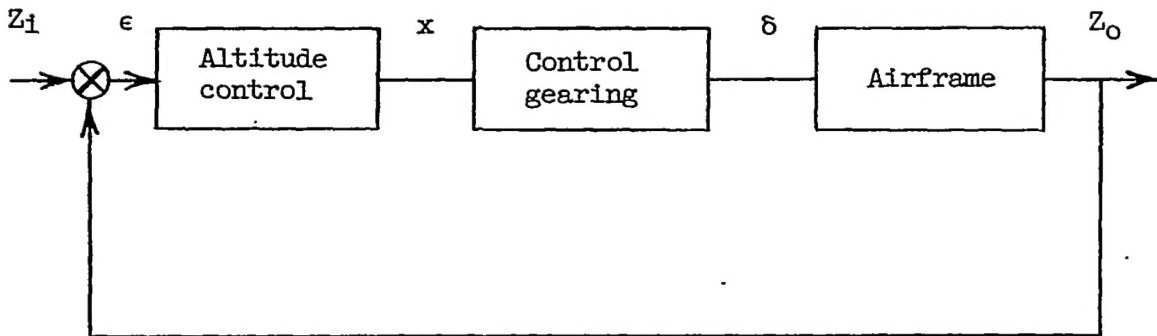
The frequency-response plot of the system shown in figure 4 was obtained through the use of a stratochamber at the Langley Instrument Research Division. In this case the altitude-control-system frequency response was measured while it was contained in the stratochamber at a simulated altitude of 40,000 feet. The sinusoidal input amplitude used for these experimental response tests was equivalent to a variation of approximately ± 480 feet at this altitude.

METHODS OF ANALYSIS

The Mach number of this analysis is 1.6, since $M = 1.6$ is considered to be average for the altitude seeking maneuvers computed herein. For the practical situation under consideration, the variation of altitude with time can be predicted by computations consisting of two main steps: (1) The initial portion would be the time history of the zero-lift trajectory based on kinematic calculations including drag, thrust, and weight variations during boosted flight, with the altitude control inactive. (2) The second step consists of the time history of the dynamic response of the missile plus altitude control including the initial-condition inputs obtained at separation. Solutions based on the foregoing can be assumed to predict the complete time response from launching to the predetermined altitude and are included in the results. In addition, the responses to a unit step input and Nyquist criterion used as a basis for component gain adjustment are included.

Servomechanism Theory

The general methods of servomechanism analysis (ref. 5) were used to evaluate the altitude control system based on the following block diagram:



Components of Block Diagram

Altitude-control block.- As mentioned previously, this block was based on experimental frequency responses of a pressure-altitude plus rate-of-climb sensing device in combination with a pneumatic servo. The gains within this combination were adjusted to allow for physically realizable control gearing adjustment.

Control-gearing block.- The choice of this ratio is dependent on space limitations, length of servo stroke, and available servo power. On this basis, the control gearing was considered to be variable within the range of approximately 0.3 to 0.5 radian per inch, since a physically realizable control-surface-servo linkage could be obtained within these values.

Airframe block.- A photograph and sketch of the actual airframe used for previous flight testing is shown in figure 5. For most of this analysis, the airframe transfer functions were obtained from a solution of the two-degree-of-freedom equations of motion. The dynamic relation between normal acceleration and δ , if two degrees of freedom are assumed, is given in reference 2 where it is pointed out that $C_{L\delta} = 0$ for the missile under consideration. The solution for Z_0/δ can then be obtained from the relation a_n/δ with the assumption:

$$Z_0 \approx \frac{a_n}{D^2} g$$

Actually the relation between vertical acceleration and normal acceleration is

$$z_o D^2 = (a_n \cos \gamma)g$$

However, the previous approximation will be valid for small values of γ .

Since a pressure sensing device such as altitude control operates at a low frequency, it was decided that the low-frequency airframe mode (phugoid) should also be included in the stability checks of the system. A portion of this analysis was therefore based on the three-degree-of-freedom airframe transfer function. The additional derivatives and the form of the three-degree-of-freedom equations of motion are contained in reference 3.

Method of Obtaining Transient Responses

Step-input responses.- Graphical procedures as outlined in reference 5 were used to obtain the closed-loop frequency response

$$\frac{z_o}{z_i} = \frac{A(j\omega)}{B(j\omega)}$$
 corresponding to zero initial conditions. The altitude

forced response $z_o(t)$ to a step-input disturbance was then obtained by the Fourier synthesizer method of transfer from the frequency domain to the time domain used previously for the analysis of reference 2. This method required the input to be expressed as a Fourier series. Each term in the series is then modified by the amplitude and phase characteristics of the closed-loop frequency response at a frequency corresponding to the term. The terms of this series are then summed with the electro-mechanical Fourier synthesizer.

In general the responses of the other variables occurring simultaneously with $z_o(t)$ and presented in the results were obtained through the use of the inverse Laplace transformation. The analytical solution was used in this case mainly because the limited number of harmonics available with the Fourier synthesizer did not permit complete definition of the motion.

Time histories of complete trajectories.- The time histories of the complete trajectories including boosted flight and the subsequent preset-altitude-seeking maneuver presented in the results were obtained by simulating the problem on a Reeves Electronic Analog Computer (REAC). For the purpose of this simulation, the block diagram was redrawn as shown in figure 6. The REAC schematics are shown within the blocks of

figure 6 and the method of obtaining the REAC schematic directly from the transfer function is presented in reference 6. The transfer function for the altitude control

$$\frac{\delta}{\epsilon} = \frac{0.782(D + 0.16)}{D^3 + 120D^2 + 5613D + 6352}$$

includes a control gearing ratio of 0.35 radian per inch and the airframe transfer function

$$\frac{\ddot{Z}}{\delta} = \frac{5000000}{D^2 + 8D + 690}$$

was obtained as mentioned previously from the relation a_n/δ given in reference 2. Solution of the problem as simulated on the REAC for the Z_0 time history was carried out as follows:

Initially a voltage proportional to the desired steady-state altitude is fed in at Z_i . This voltage feeds through the first block (the altitude control) to produce a signal at δ . The open switch at δ , however, stops the signal at this point. This simulates the missile on the ground prior to launching with the altitude control preset to the desired steady-state altitude and the control surface locked at zero. The control surface is locked because no deflections can be tolerated during boosted flight for structural reasons. However, at missile-booster separation the control surface will be unlocked through a switching device and δ will rapidly assume the value that is dictated by the error feeding through the dynamics of the controlling elements at that instant. The problem of unlocking the control at the instant of separation is simulated in the REAC setup (fig. 6) simply by closing the switch between the first and second blocks.

The second block of figure 6 represents the airframe transfer function \ddot{Z}/δ . The initial condition (ic) on the second integrator within this block is equal to the value of voltage proportional to \ddot{Z} of the missile alone the instant separation from the booster is achieved. The switch in the outer loop of the \ddot{Z}/δ schematic prevents the initial condition from influencing the balance of the airframe schematic during the simulation of boosted flight.

Boosted flight is simulated by feeding a voltage proportional to \ddot{Z} through the switch between the second and third blocks of figure 6. This

voltage is the output of a function generator for which the plot of \ddot{Z} against time was obtained from kinematic computations by utilizing the relation

$$\ddot{Z} = \left(\frac{\text{Thrust} - \text{Drag}}{\text{Weight}} \sin \gamma - 1 \right) 32.2$$

The voltage proportional to \ddot{Z} is shown to feed through two integrator blocks to yield Z_0 . Then Z_0 is fed back during boosted flight and is compared with Z_1 in accordance with the relation

$$Z_1 - Z_0 = \epsilon$$

At the instant of separation (3.2 seconds), the three switches close through the use of a relay amplifier and the problem is allowed to run until Z_0 steadies out at the value corresponding to Z_1 .

RESULTS AND DISCUSSION

System Stability and Responses

Nyquist diagrams.- Figure 7 shows the Nyquist diagram of the open loop Z_0/ϵ with the gain K_{cg} set at 0.35 radian per inch for sea-level flight conditions at $M = 1.6$ with the airframe transfer function based on two degrees of freedom. The phase margin at which the locus crosses the 0 db or $AR = 1$ circle is approximately 44° which indicates adequate stability. This phase margin is obtained by the rate-of-climb sensing of the altitude control since the altitude-control frequency response (fig. 3) shows leading phase characteristics between the frequency range of 0.01 to 6 radians per second. With decreasing frequency, the locus of Z_0/ϵ is tending toward -180° , as can be seen in figure 7. This is caused by the double integration in the airframe transfer function Z_0/δ which occurs due to the assumption

$$Z_0 = \frac{a_n}{D^2} g$$

This implies that the altitude control system is a servomechanism which has neither steady-state position or velocity error as discussed in reference 7 but would be unstable without leading phase characteristics

since it has a zero-frequency open-loop phase relation of -180° and, except for the rate-of-climb sensing, the balance of the dynamics of the system has lagging characteristics.

In figure 8 the results of an analysis of the altitude control system in which the airframe transfer function is based on three degrees of freedom is shown in the form of Nyquist plots. The results of reference 3 which include the effect of velocity derivatives were employed in obtaining the three-degree-of-freedom airframe transfer functions. In figure 8 the stability is investigated at trim angle-of-attack values of 0° , 4° , and 10° for an assumed equilibrium Mach number of $M = 1.6$ and constant control-system component gains. This approach (that is, making stability checks at more than one trim angle of attack) is discussed in reference 3. The locus obtained for 0° angle of attack in figure 8 is shown to be the same as the locus shown in figure 7. The locii shown for angle-of-attack values of 4° and 10° , however, are shown to deviate somewhat from the 0° angle-of-attack locus. These deviations are due to the additional airframe dynamics arising from the increase in degrees of freedom. The open-loop locii also show an increase in phase margin for the higher angle-of-attack values because the lead terms of the airframe transfer function actually break at lower frequencies than the phugoid quadratic. This increase in phase margin indicates an increase in system stability or more heavily damped closed-loop response. Therefore, basing the analysis of a control system of this type on two-degree-of-freedom solution is considered to be sufficient, since the control-system gain adjustment is more critical in this instance.

Step-input responses at sea level. -- The Z_o transient response to a unit step input Z_i is shown in figure 9. The flight conditions and gain adjustment are the same as used previously for the Nyquist diagram (fig. 7). The Z_o response is shown to have approximately 1.3 overshoot and remains within 5 percent of steady state after 6.3 seconds. Figure 9 also shows the a_n , δ , θ , γ , and α responses which occur simultaneously with the Z_o response to a unit step Z_i input. The peak values of these responses are important in the altitude control application. In particular, there are structural limitations on the maximum normal acceleration and the accuracy of the transient solution is governed by the magnitude of γ . The peak values of these additional variables obtained from figure 9 are tabulated as follows:

Variable	Unit-step peak value	500-ft-step peak value
a_n , g units	0.048	24
δ , deg	.0076	3.8
θ , deg	.0195	9.8
γ , deg	.019	9.5
α , deg	.011	5.5

The peak normal acceleration of 24 g units obtained for the 500-foot step is within the design load limit of the missile, and the inaccuracies introduced with the assumption

$$Z_0 = \frac{a_n}{D^2} g$$

are not considered serious since the flight-path-angle variations are within 10° during the altitude-seeking maneuver based on the 500-foot step input.

Step-input response at 40,000 feet. - The Z_0 response to a unit step input Z_1 obtained for the 40,000-foot-altitude case is shown in figure 10. This response is based on the altitude-control frequency response shown previously in figure 4 obtained in a stratochamber at the Langley Instrument Research Division at a simulated altitude of 40,000 feet combined with the solution for the airframe transfer function at the same simulated altitude. A comparison of the 40,000-foot and sea-level responses indicates that the 40,000-foot response exhibits an increase in peak overshoot of approximately 10 percent and the time to reach and remain within 5 percent of steady state is increased by about 30 percent. Figure 10, however, does indicate that the altitude control system can be made to function successfully at high altitude, since the response at altitude is very similar to the sea-level response (fig. 9).

Predicted Time History of Complete Trajectories

Time histories of complete trajectories including boosted flight and the subsequent automatic altitude-seeking maneuver as obtained from REAC simulation of the problem are presented in figure 11. Figure 11(a) shows the time histories for launching angles of 20° and 30° with Z_1 preset at a steady-state value equal to the separation altitude plus 500 feet. Figure 11(b) shows time histories for the same launching angles with Z_1 preset at a steady-state value equal to the separation altitude plus

250 feet. For the cases shown, no overshoot is obtained with the 20° launching angle and altitude stabilization is particularly poor with the larger steady-state altitude (fig. 11(a)) whereas for the 30° launching angle the initial overshoot obtained is higher for the lower steady-state value (fig. 11(b)). The overshoot obtained with the larger launching angle is due to the higher rate of climb obtained at separation in this instance. In general it can be seen that the ability to reach and stabilize about a desired altitude is governed mainly by two factors (the magnitude of the preset altitude and the launching angle), and for the problem under consideration, altitude stabilization will be improved by the choice of launching angle which yields some initial overshoot. The control-surface responses during the altitude-seeking maneuver are also shown in figure 11. It is noted that δ immediately assumes a negative value at missile-booster separation. This negative value indicates that the rate of climb obtained during boosted flight is feeding a larger signal to the control surface than Z_1 by the time separation is achieved.

It is apparent particularly for a launching angle of 30° that the initial overshoot is decreased by increasing the steady-state altitude (see fig. 11). The initial overshoot could also be decreased by delaying the altitude-control activation and leveling off at a still higher altitude; however, for the boost-glide missile under consideration the price paid in loss of Mach number would be great. For application to long-range missiles where thrust is available in the second stage, loss of Mach number would not be a problem. The launching angle and delay in control-surface actuation could be selected so that the desired steady-state altitude would be the peak of the zero-lift trajectory. In this instance there would be no initial inputs to the control system to generate oscillations such as those shown for a 30° launching angle in figure 11. The curves of figure 11, however, show the altitude control system to be a workable system since it will seek and tends to remain at a predetermined altitude.

Effect of Aerodynamic Out-of-Trim Moment or Load Disturbance

In reference 2 it is pointed out that an aerodynamic out-of-trim moment may be represented by an equivalent control-surface deflection. If this approach is taken for the present analysis, it can be seen that the steady-state Z_0 error due to an equivalent control-surface deflection is the inverse of the static gain of the controlling elements. Since the static gain of the altitude control was necessarily set quite low for reasons of stability, the resultant overall system may have a fairly large steady-state error when viewed from the standpoint of out-of-trim moment and from the load-disturbance standpoint it will be a fairly loose control system. For example, if the aerodynamic out-of-trim moment due to model misalignment is assumed to be equivalent to a

control-surface deflection of 0.25° , the steady-state Z_0 error will be approximately 220 feet for the low-altitude case. This error will be increased for flight at a 40,000 foot altitude to about 1,000 feet (note the apparent decrease in static gain when the altitude-control frequency response is measured at a simulated altitude of 40,000 feet shown in fig. 4 as compared to the sea-level static gain of fig. 2).

Load disturbances (for instance disturbances due to vertical gusts) are sometimes considered to be time-variant moments which can also be represented by equivalent control-surface deflections. No attempt is made here to determine the effect of a fixed magnitude and frequency gust spectrum on the control-system response. However, in the presence of gusty conditions, it is evident that the missile would tend to wander about its reference altitude to a certain extent due to the looseness of control brought about by the low static gain of the control elements.

CONCLUDING REMARKS

When the altitude control is analyzed in combination with the airframe transfer function based on two degrees of freedom or three degrees of freedom at zero trim angle of attack, the open-loop frequency response contains a double integration and the airframe does not contribute any dynamic lead. Therefore the lead obtained with rate-of-climb sensing is necessary in order to obtain a stable system.

The altitude-control-system response to a step input at 40,000 feet is somewhat slower and has slightly more initial overshoot than the response at sea-level; however, the response obtained at altitude is very similar to the sea-level response and it is concluded that the system can be made to function successfully at high altitude.

The predicted time histories of the trajectories obtained with a 30° launching angle show the altitude-seeking maneuver to be somewhat oscillatory for the boost-glide missile under consideration. The problem simulated, however, is only for evaluation purposes and is more severe than that which would be encountered with a two-stage missile where thrust was available for the second stage.

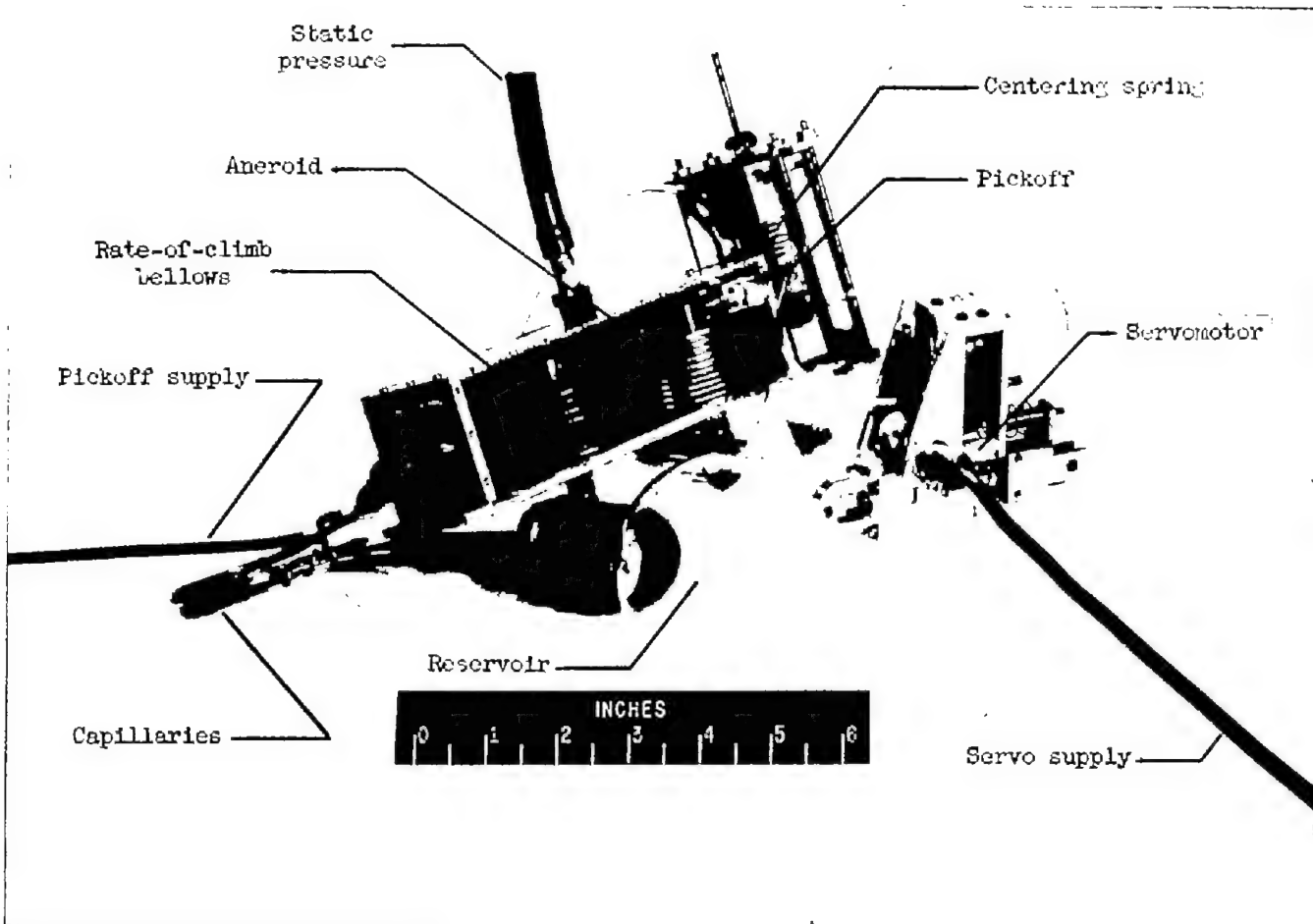
In the presence of model misalignment, the steady-state altitude error due to the resulting aerodynamic out-of-trim moment may be quite large. This steady-state error is large in the altitude control application because it is inversely proportional to the static gain of the altitude-control transfer function which was necessarily set quite low for reasons of stability. This low static gain will cause the altitude

control to be a relatively loose system. The missile will therefore tend to wander about its reference altitude to a certain extent in the presence of gusty conditions.

Langley Aeronautical Laboratory,
National Advisory Committee for Aeronautics,
Langley Field, Va., May 25, 1954.

REFERENCES

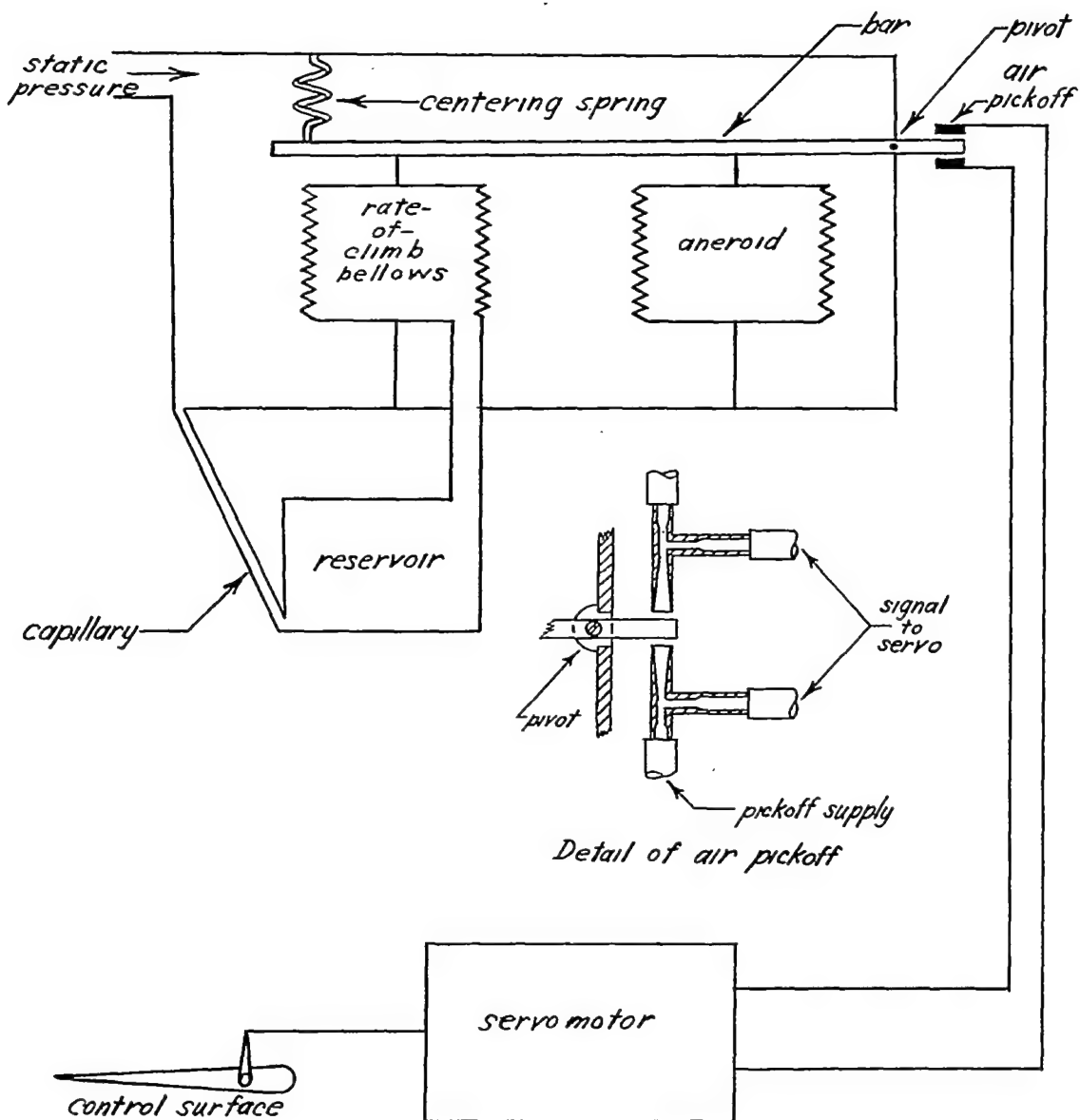
1. Zarovsky, Jacob, and Gardiner, Robert A.: Flight Investigation of a Roll-Stabilized Missile Configuration at Varying Angles of Attack at Mach Numbers Between 0.8 and 1.79. NACA RM L50H21, 1951.
2. Seaberg, Ernest C., and Smith, Earl F.: Theoretical Investigation of an Automatic Control System With Primary Sensitivity to Normal Accelerations as Used To Control a Supersonic Canard Missile Configuration. NACA RM L51D23, 1951.
3. Seaberg, Ernest C.: Three-Degree-of-Freedom Evaluation of the Longitudinal Transfer Functions of a Supersonic Canard Missile Configuration Including Changes in Forward Speed. NACA RM L54C02, 1954.
4. Seaberg, Ernest C.: Theoretical Investigation of a Proportional-Plus-Flicker Automatic Pilot. NACA RM L50I19, 1950.
5. Brown, Gordon S., and Campbell, Donald P.: Principles of Servomechanisms. John Wiley & Sons, Inc., 1948.
6. Beck, C.: A Method for Solving Problems on the REAC by the Use of Transfer Functions Without Passive Networks. Paper No. 18 of Project Cyclone Symposium I on REAC Techniques, Reeves Instrument Corp. (New York City), Mar. 15-16, 1951, pp. 131-136.
7. Chestnut, Harold, and Mayer, Robert W.: Servomechanisms and Regulating System Design. Vol. I. John Wiley & Sons, Inc., 1951.



(a) Photograph of altitude control.

L-82435.1

Figure 1.- Photograph and schematic diagram of altitude control.



(b) Schematic diagram of altitude control.

Figure 1.- Concluded.

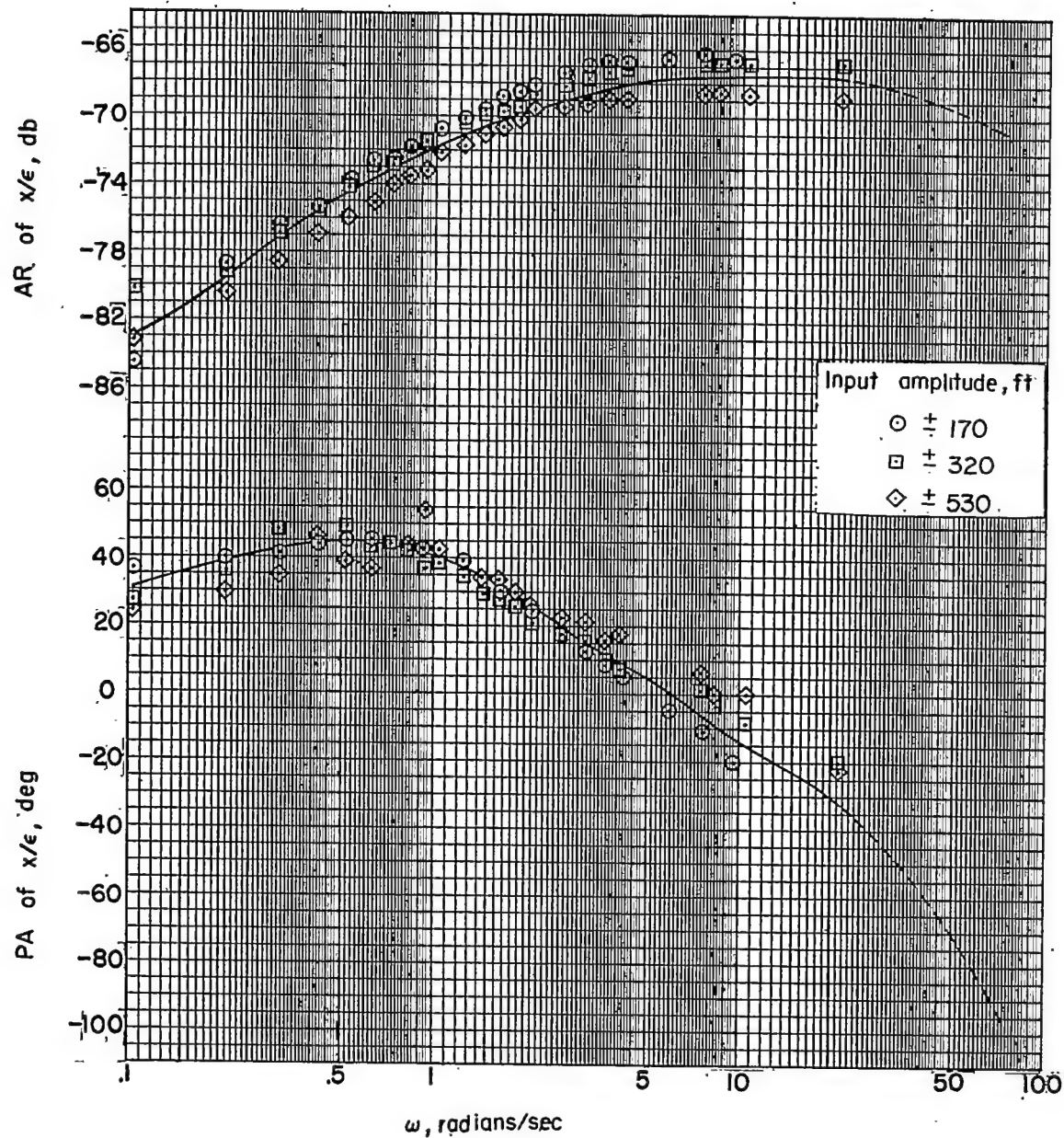


Figure 2.- Experimental frequency response of altitude control obtained at sea level for three input amplitudes.

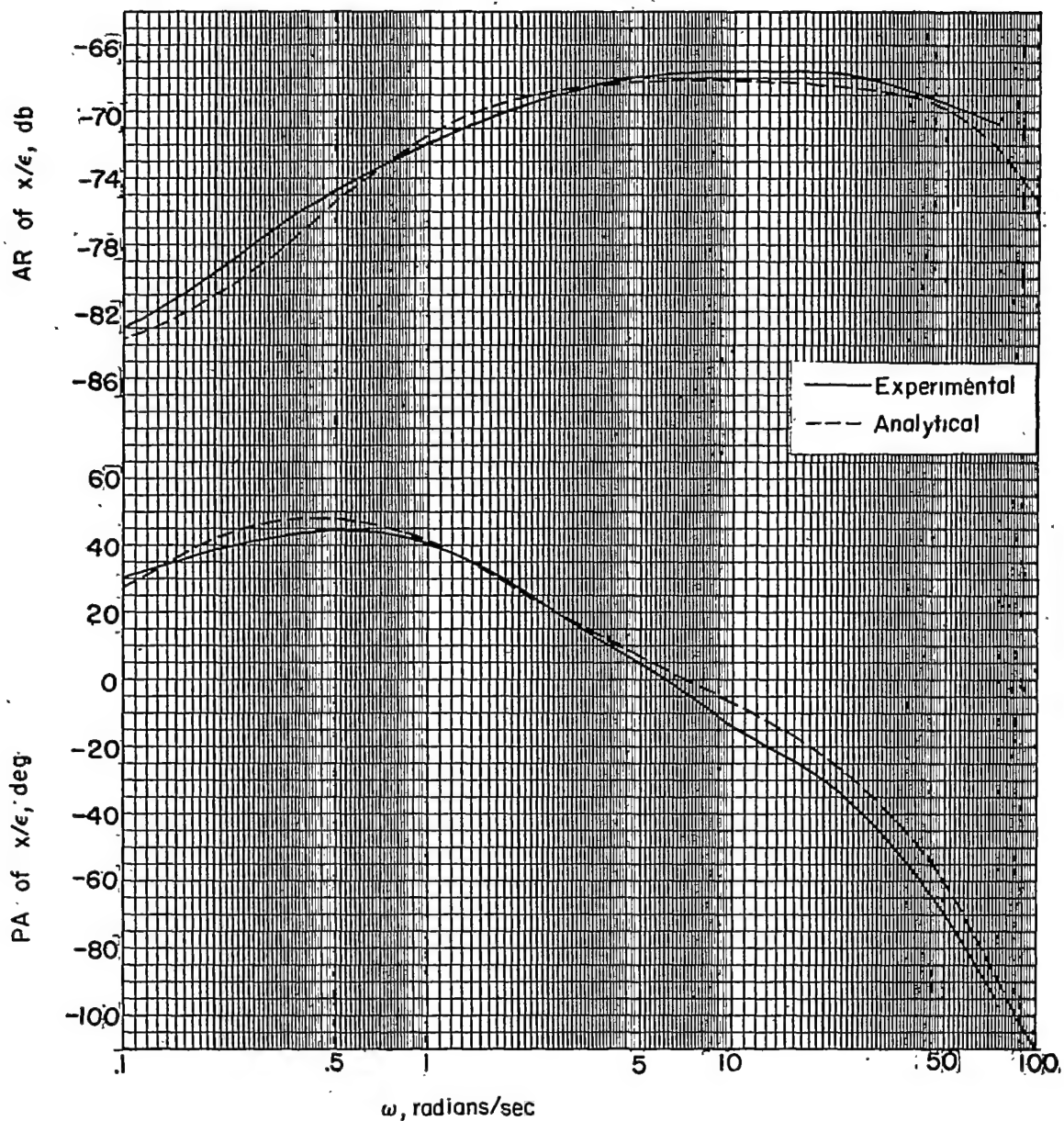


Figure 3.- Comparison between faired experimental frequency-response curve and approximate analytical frequency-response curve.

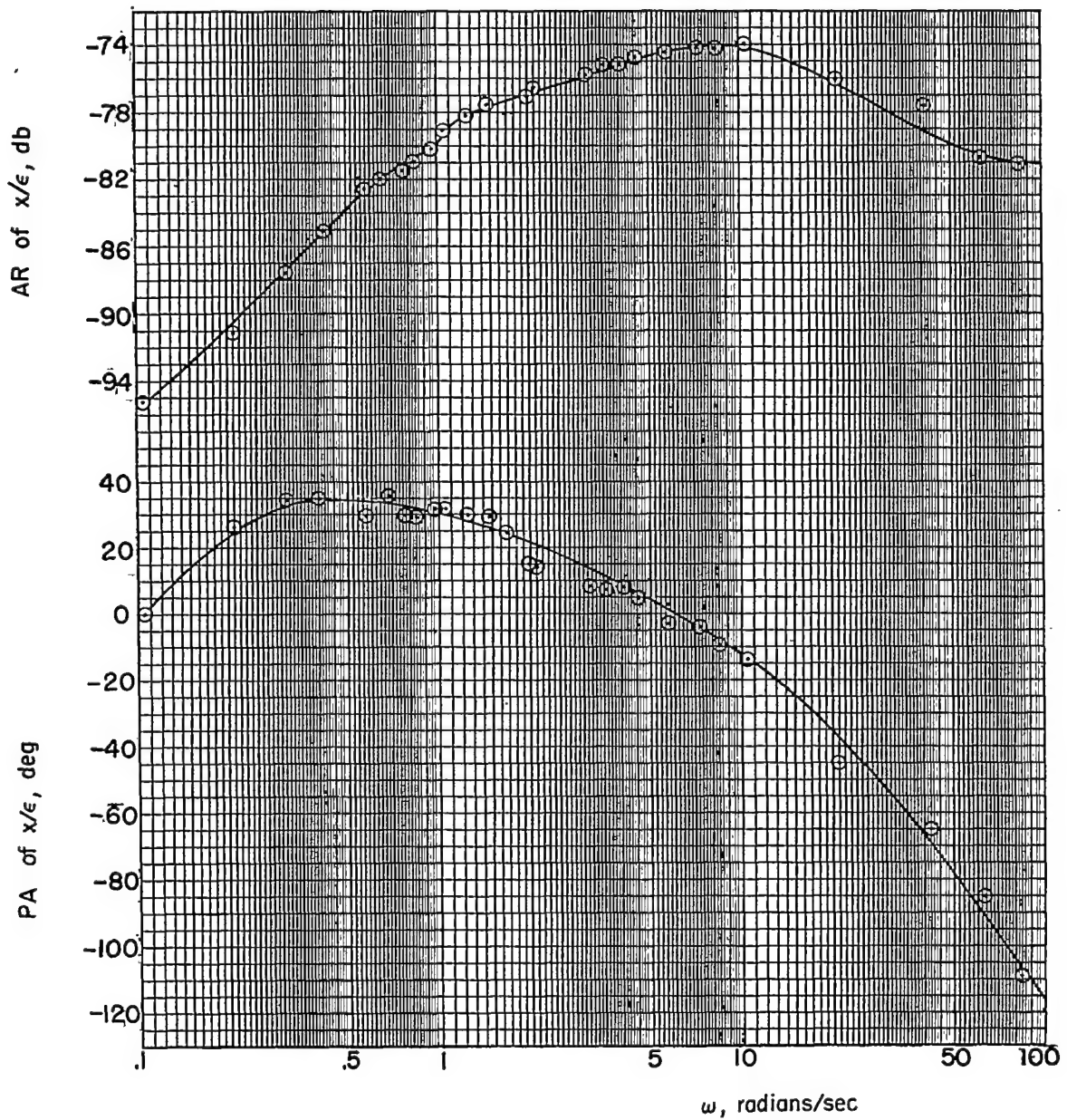
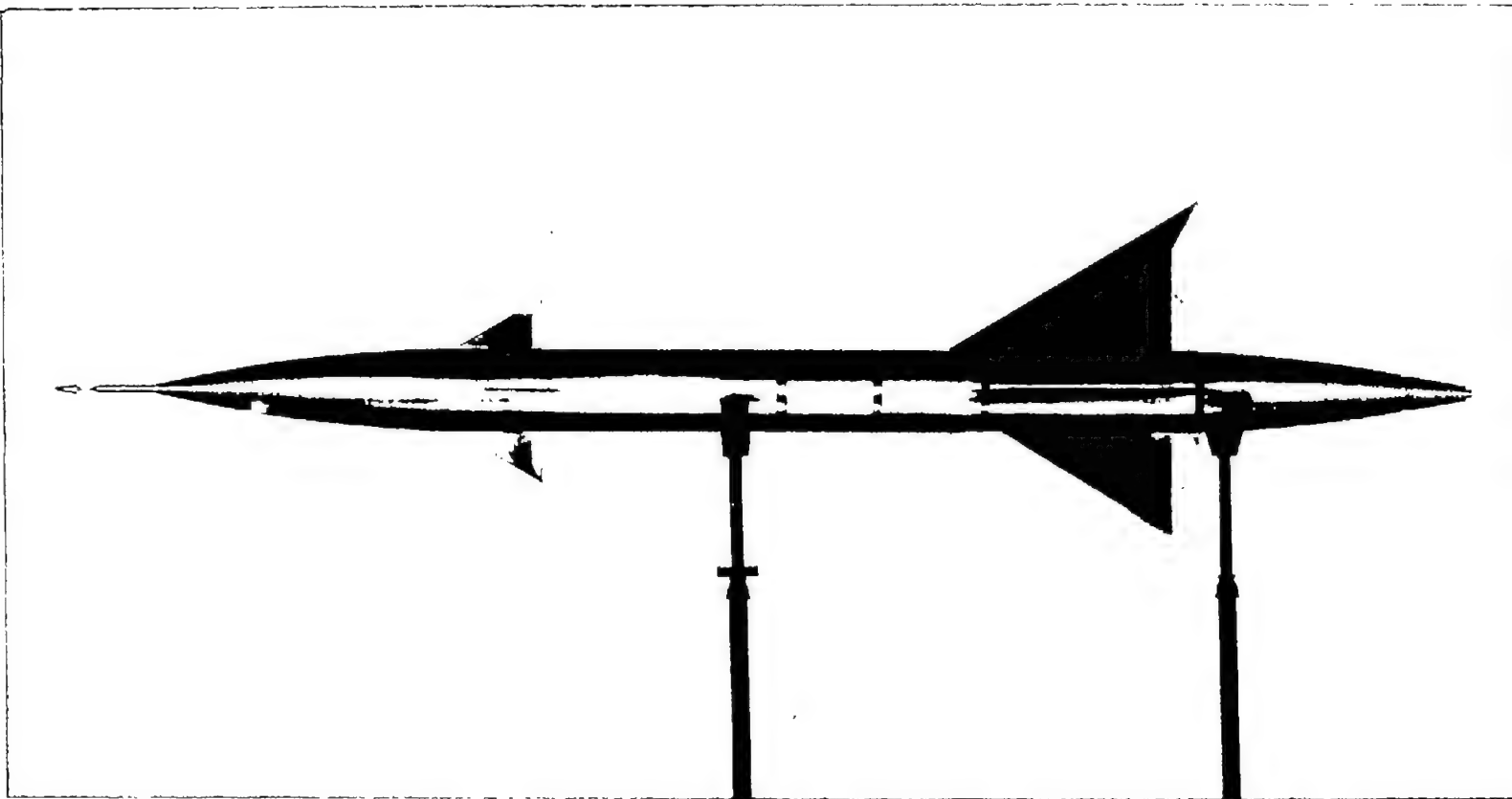


Figure 4.- Experimental frequency response of altitude control obtained for simulated 40,000-foot altitude. Input amplitude, ± 480 feet.

CONFIDENTIAL

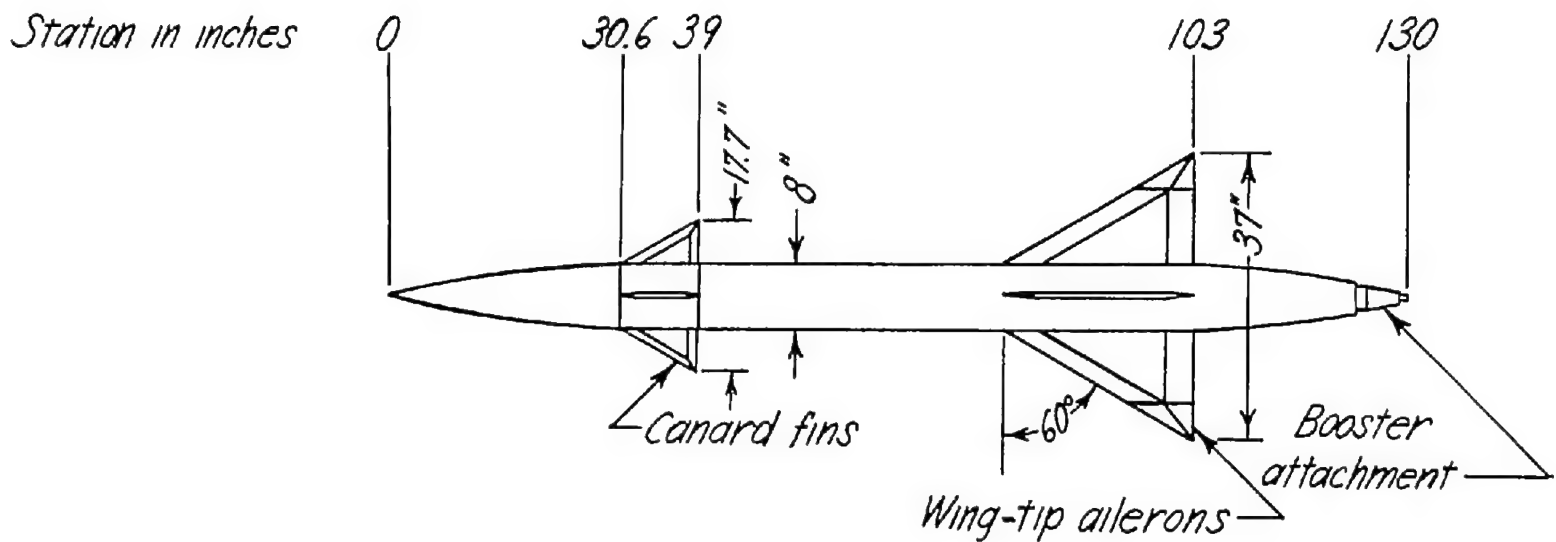
NACA RM 154FO4



L-67712.1

(a) Photograph of model configuration.

Figure 5.- Supersonic missile research model configuration.



(b) Plan-view sketch of model configuration.

Figure 5.- Concluded.

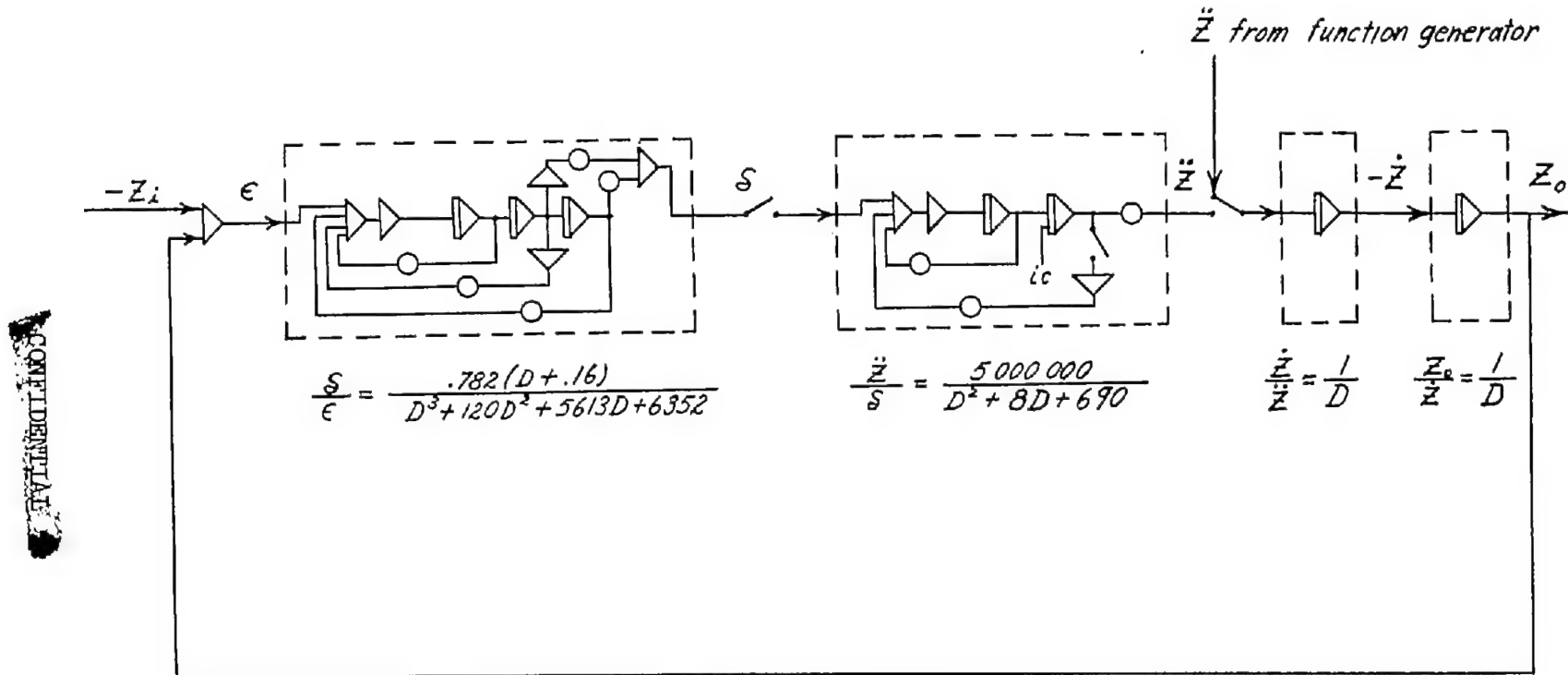


Figure 6-- Block diagram of altitude control system showing the schematic setup used in simulating the time histories of the complete trajectories. Switches are shown in the position for simulating boosted flight.
 $K_{cg} = 0.35$ radian per inch.

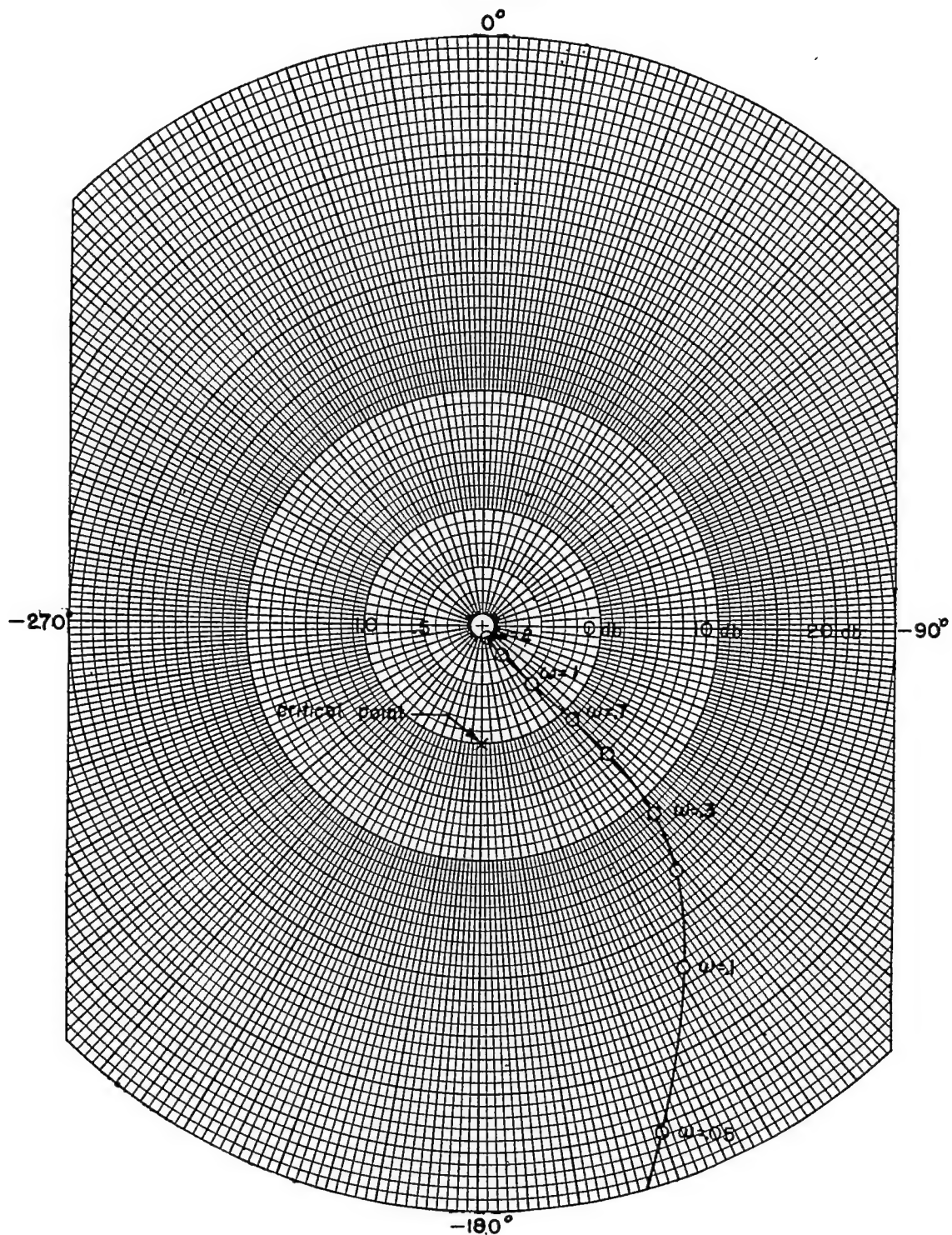


Figure 7.- Nyquist diagram Z_o/ϵ for altitude control system with $K_{cg} = 0.35$ radian per inch for sea-level flight conditions at $M = 1.6$, $x_{sm} = 0.294\bar{c}$.

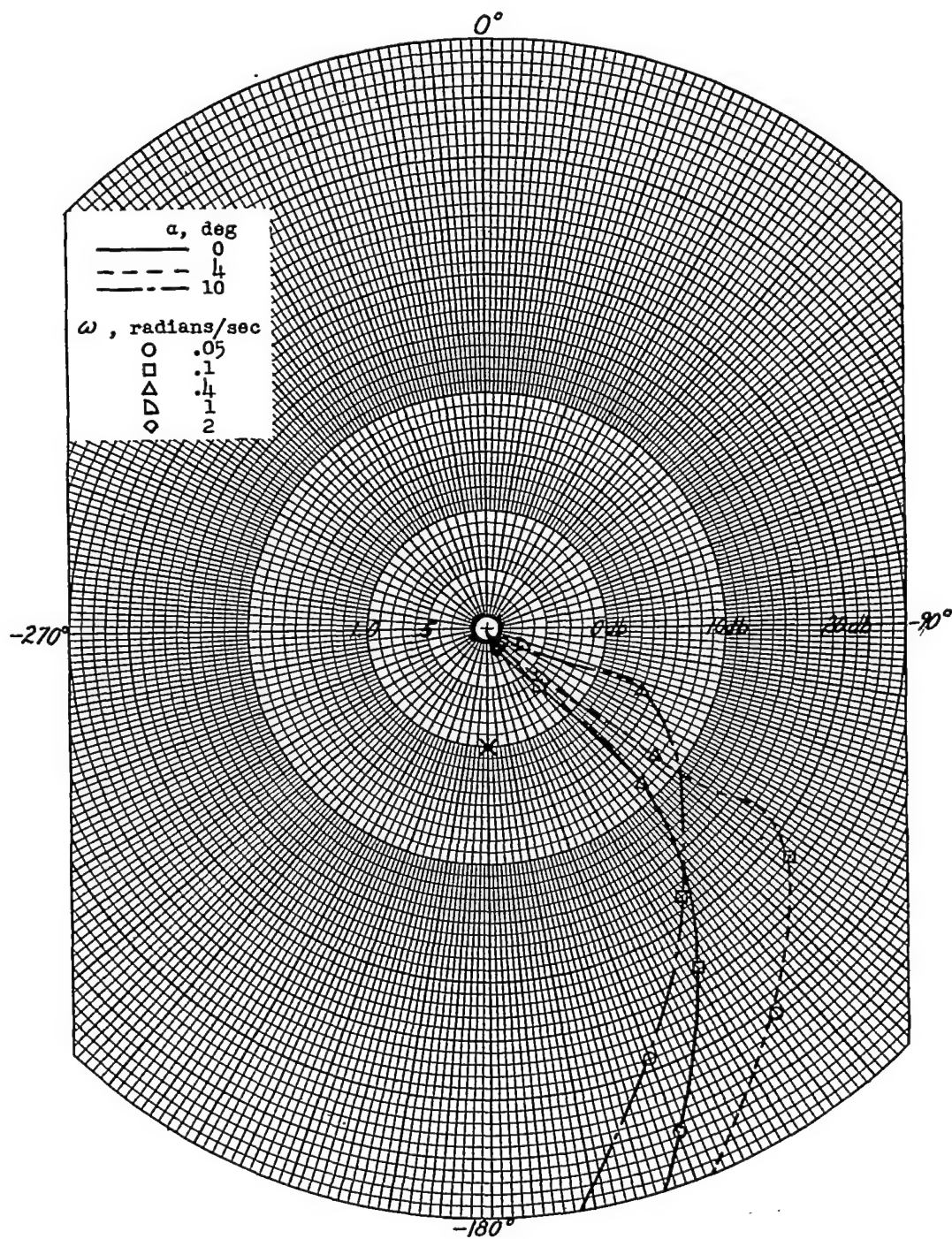


Figure 8.- Nyquist diagrams Z_0/ϵ for altitude control system with air-frame transfer function Z_0/δ based on three degrees of freedom and for angle-of-attack values of 0° , 4° , and 10° . $K_{cg} = 0.35$ radian per inch; sea-level conditions; $M = 1.6$; $x_{sm} = 0.294c$.

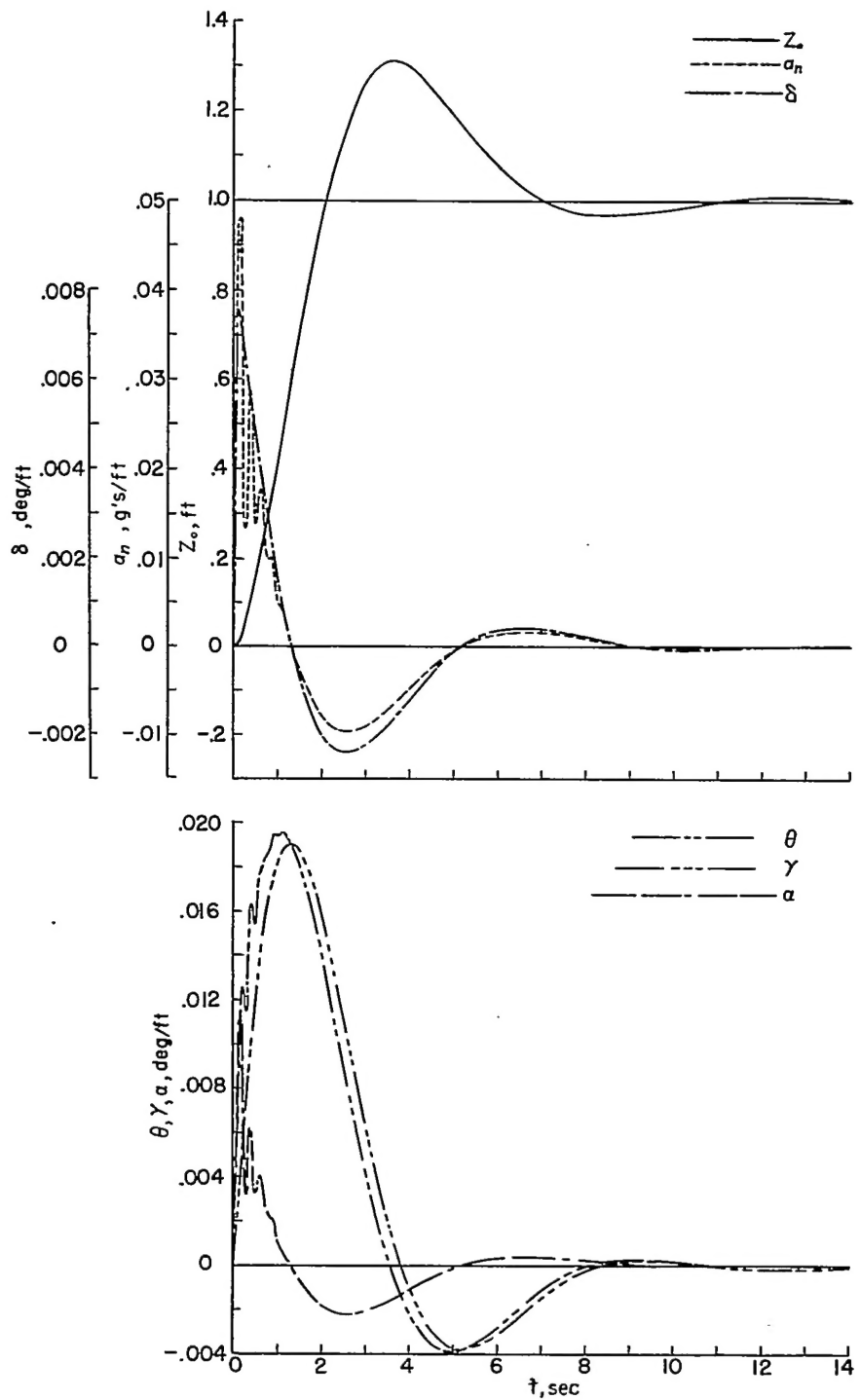


Figure 9.- Z_o , a_n , δ , θ , γ , and α transient responses to a unit step altitude input for sea-level flight conditions at $M = 1.6$, $x_{sm} = 0.294\bar{c}$, $K_{cg} = 0.35$ radian per inch.

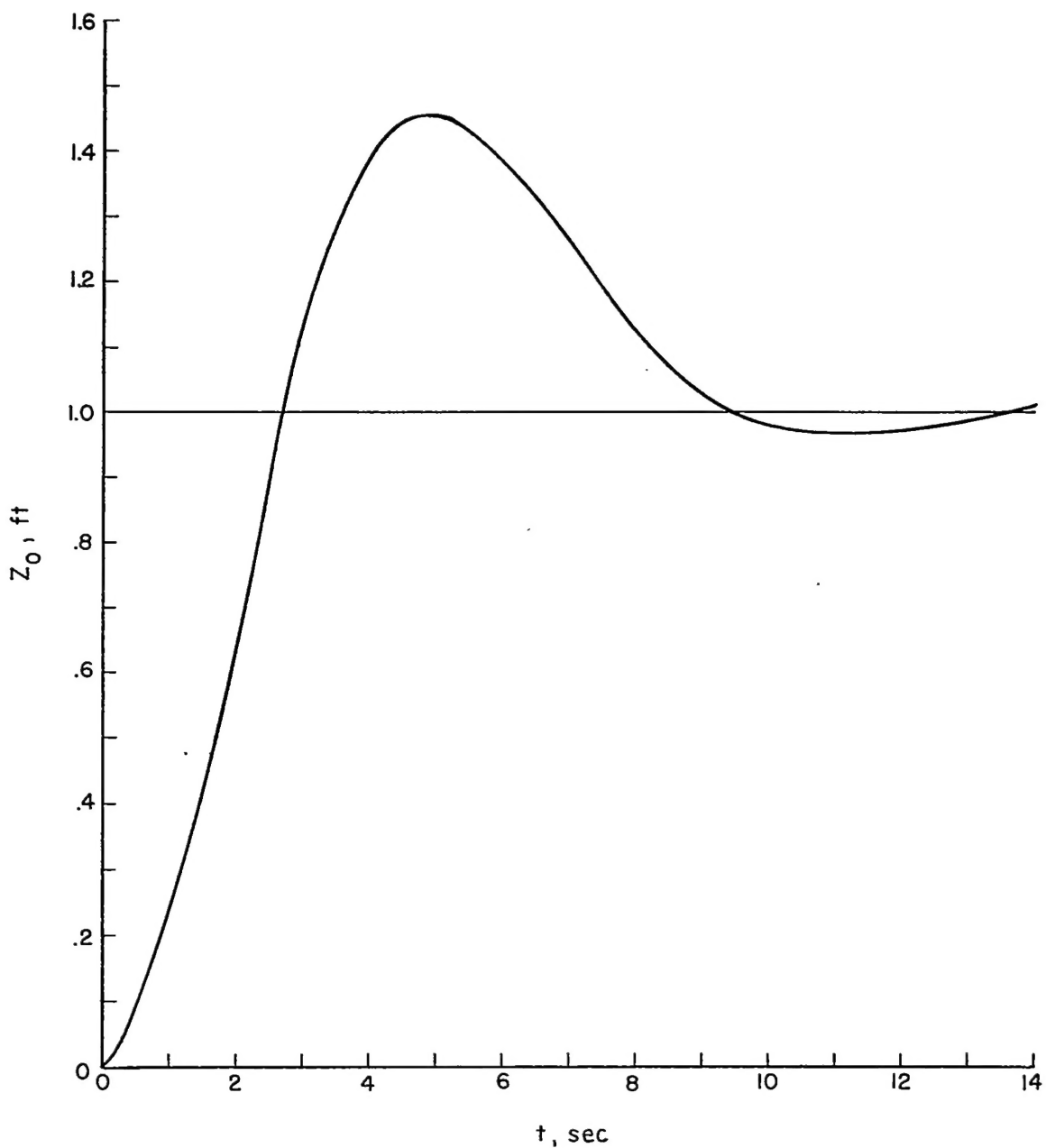
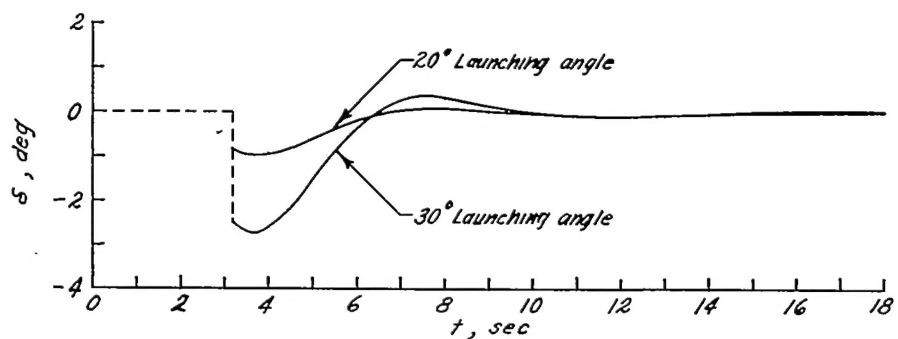
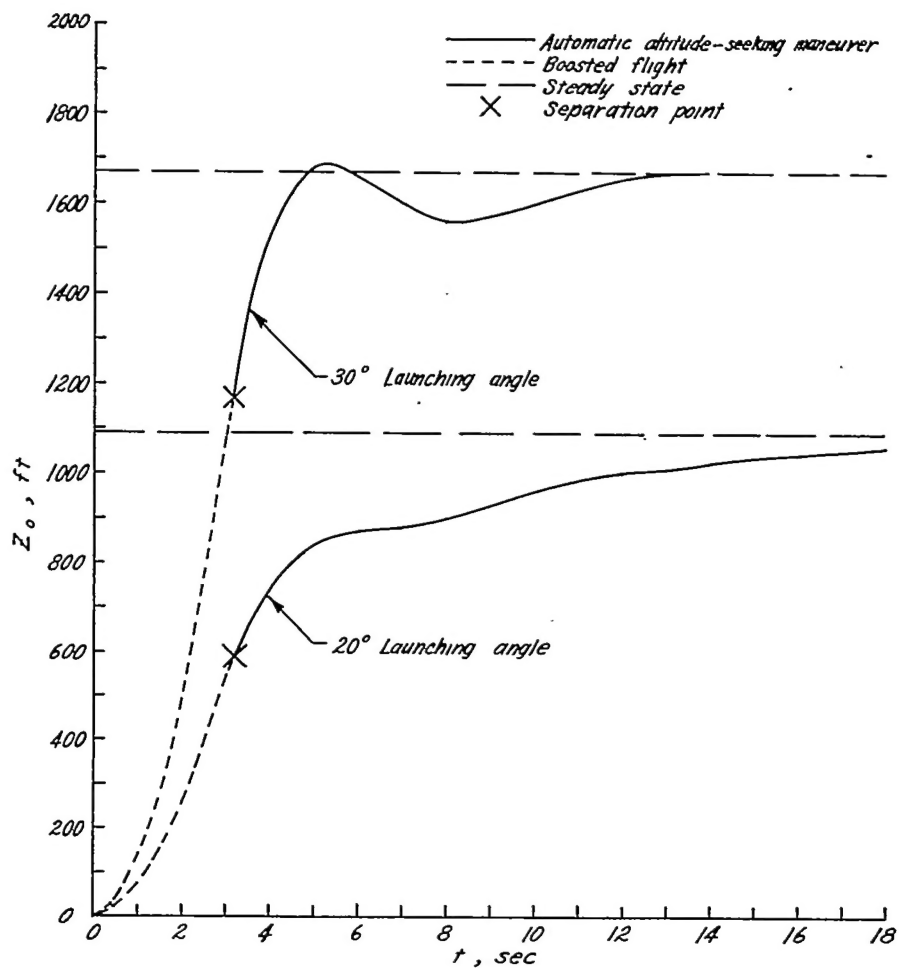


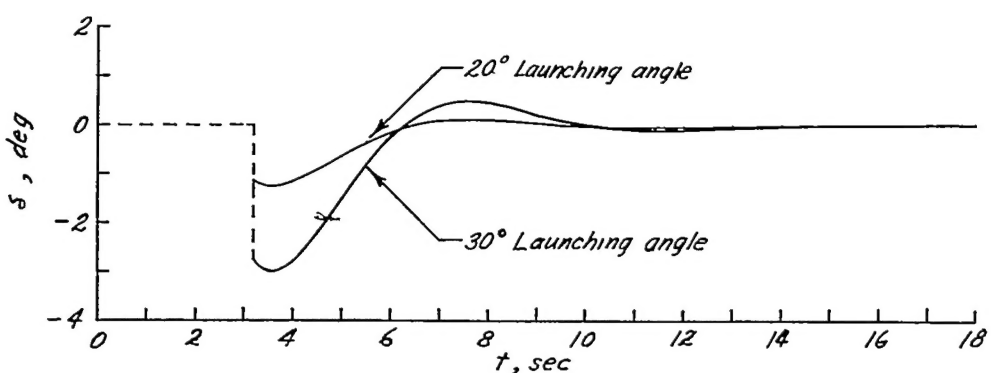
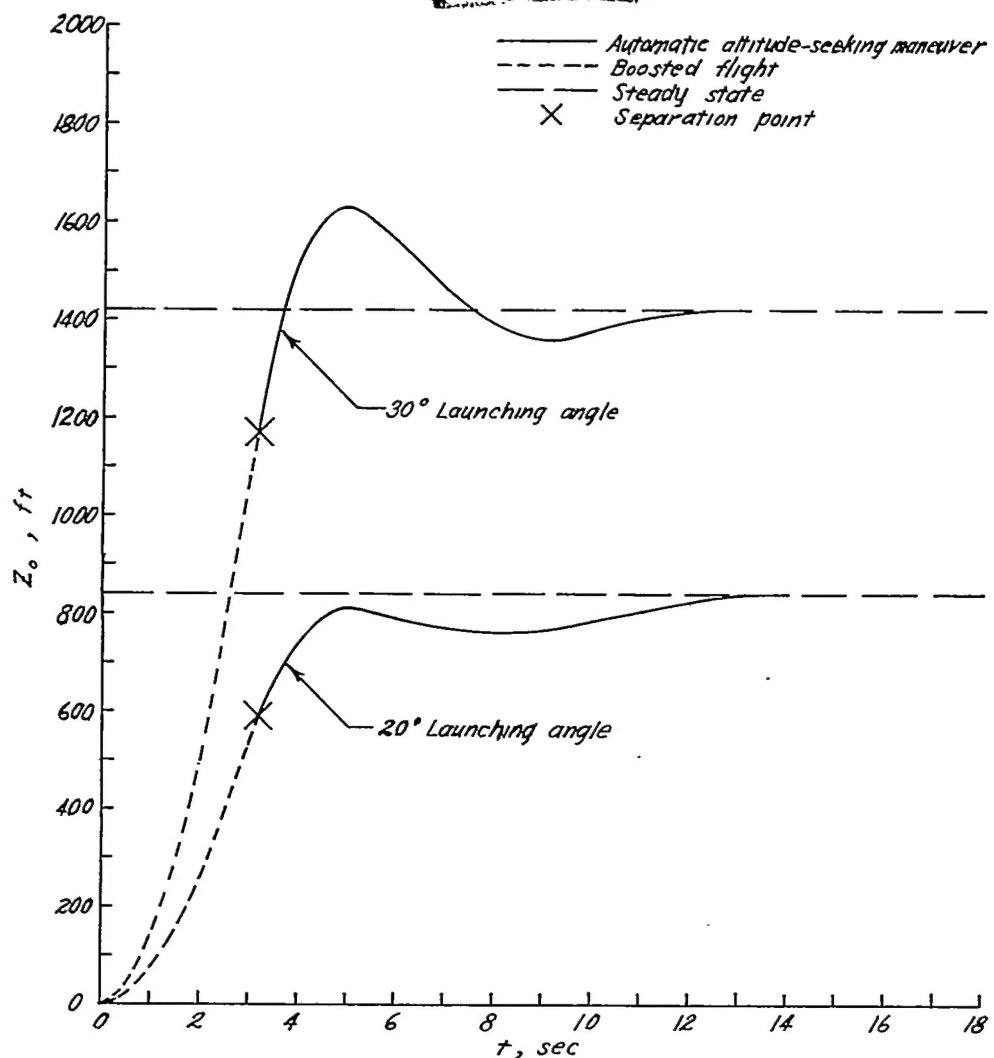
Figure 10.- Z_0 transient response to a unit step altitude input based on flight at 40,000 feet and $M = 1.6$. $K_{cg} = 0.35$ radian per inch.



(a) $Z_1 = \text{Separation altitude} + 500 \text{ feet.}$

Figure 11.- Time histories of complete trajectories including boosted flight and subsequent automatic altitude-seeking maneuver. Comparison is made between trajectories for 20° and 30° launching angles for sea-level flight conditions at $M = 1.6$; $x_{sm} = 0.294\bar{c}$; $K_{cg} = 0.35$ radian per inch.

CONFIDENTIAL



(b) Z_1 = Separation altitude + 250 feet.

Figure 11.- Concluded.

CONFIDENTIAL